



HAL
open science

Vibration and luminosity frequency analysis of the SuperKEKB collider

Maurizio Serluca, Gael Balik, Laurent Brunetti, Benjamin Aimard, Agnes Dominjon, Philip Bambade, Sandry Wallon, Salvatore Di Carlo, Mika Masuzawa, Sadaharu Uehara

► **To cite this version:**

Maurizio Serluca, Gael Balik, Laurent Brunetti, Benjamin Aimard, Agnes Dominjon, et al.. Vibration and luminosity frequency analysis of the SuperKEKB collider. Nucl.Instrum.Meth.A, 2022, 1025, pp.166123. 10.1016/j.nima.2021.166123. hal-03520514

HAL Id: hal-03520514

<https://hal.science/hal-03520514>

Submitted on 8 Jan 2024

HAL is a multi-disciplinary open access archive for the deposit and dissemination of scientific research documents, whether they are published or not. The documents may come from teaching and research institutions in France or abroad, or from public or private research centers.

L'archive ouverte pluridisciplinaire **HAL**, est destinée au dépôt et à la diffusion de documents scientifiques de niveau recherche, publiés ou non, émanant des établissements d'enseignement et de recherche français ou étrangers, des laboratoires publics ou privés.



Distributed under a Creative Commons Attribution - NonCommercial 4.0 International License

Vibration and Luminosity Frequency Analysis of the SuperKEKB Collider

Maurizio Serluca^a, Gael Balik^a, Laurent Brunetti^{a,*}, Benjamin Aimard^a,
Agnes Dominjon^a, Philip Bambade^b, Sandry Wallon^b, Salvatore Di Carlo^c,
Mika Masuzawa^d, Sadaharu Uehara^d

^a*Univ. Savoie Mont Blanc, CNRS, Laboratoire d'Annecy de Physique des Particules - IN2P3, 74000 Annecy, France*

^b*Laboratoire de Physique des 2 Infinis Irène Joliot Curie, 15 Rue Georges Clemenceau, 91400 Orsay, France*

^c*CERN, Espl. des Particules 1, 1211 Meyrin, Switzerland*

^d*KEK, 1-1 Oho, Tsukuba, Ibaraki 305-0801, Japan*

Abstract

The SuperKEKB collider has entered the physics production phase with the aim to reach its target luminosity of $6 \times 10^{35} \text{cm}^{-2}\text{s}^{-1}$. Vibrations of the accelerator elements, especially around the Interaction Point (IP), could limit the performance of the collider. Since 2018, a 24-hour monitoring system of vibrations has been put in place on both sides of the Belle II detector. Measurements and analyses of the spectral components of these vibrations and of the transfer function of the mechanical supports are presented, along with measurements of luminosity spectra from the LumiBelle2 detectors, showing good agreement in spectral peak frequencies for several of the vibration sources.

Keywords: SuperKEKB, ground motion, mechanical vibrations, Lumibelle2

2010 MSC: 00-01, 99-00

1. Introduction

SuperKEKB is the last generation of B-factory machines designed to achieve a peak luminosity 40 times higher than that of KEKB. In the *nanobeam* collision scheme, the vertical size of the beam is squeezed down to few tens of nm at the

*Corresponding author

Email address: laurent.brunetti@lapp.in2p3.fr (Laurent Brunetti)

5 IP thanks to the superconducting (SC) final focus system mounted in cantilever mode and inserted inside the detector [1]. Since the 15th of June 2020, SuperKEKB has achieved the world's highest luminosity for an electron-positron collider and keeps pushing it towards the target luminosity. The vibrations of final focus quadrupoles induce an orbit distortion at the IP that could be larger
10 than the vertical beam size. In this context, countermeasures have been taken to ensure the optimal collision conditions such as special care for the mechanical design of the final focus cryostats and their supports, vibration measurements in the detector area and implementation of feedback systems [2, 3].

15 After a first vibration measuring campaign performed on the cryostat of the final focus system (front side of the Belle II detector) post mechanical assembly, a second campaign was carried out in November 2018. Two seismic sensors were added on the floor on both sides of the detector to monitor vibrations. In December 2018, the 24 hours monitoring system was upgraded with the further
20 installation of two more sensors placed on the tables of the mechanical supports on both sides of the final focus system.

The LumiBelle2 fast luminosity monitoring system is based on diamond sensors installed in both the electron and positron beamlines, called High Energy
25 Ring (HER) with electrons at 7 GeV and Low Energy Ring (LER) with positrons at 4 GeV [4]. Another monitoring system, the Zero Degree Luminosity Monitor (ZDLM), using Cherenkov and scintillator detectors[5], is also installed at the same locations, very close to the LumiBelle2 sensors, and provides complementary information.

30 SuperKEKB has two IP feedback systems to ensure optimal collision conditions. The horizontal IP feedback system has been changed from the beam-beam deflection based system of KEKB [6] to a dithering system similar to the one used at the SLAC PEP-II collider [7, 8]. The vertical IP feedback system is based on the beam-beam deflection method and uses four Beam Position Mon-
35 itors (BPM) installed on both sides of the IP, near the final focus quadrupoles

(QC1RE, QC1RP, QC1LE, QC1LP), in order to drive the associated correction kickers [3].

Data acquired from seismic sensors during the phase 3 commissioning in
40 2019 and during the physics run in 2020 have been analysed to identify vibra-
tion sources and to evaluate relevant transfer functions of mechanical supports,
spatial coherence through backside-frontside asymmetries, the frequency com-
ponents introduced by technical-cultural noise, and their variation in time. The
monitoring system is always active while data are recorded 10 minutes per hour
45 to reduce the amount of data to be stored. Luminosity data in the same time
intervals are recorded for the four channels of LumiBelle2 and analysed to study
the possible correspondence in frequency among the luminosity and mechanical
vibration signals. A continuously updated status report of the vibration mea-
surements is provided [9].

50

Vibrations of focusing magnets induce orbit distortion of the two beams,
which could be particularly important for the strongest quadrupoles of the final
focus system depending on the spatial coherence of the vibrations, the lon-
gitudinal position of the quadrupoles and the amplitude amplification of the
55 mechanical structures frequency resonances. Furthermore, in SuperKEKB the
different energy of the two beams along with the different mechanical design and
weight of the two cryostats mounted in cantilever mode conspire in a complex
way to yield the beam orbit separation at the IP.

Assuming a perfect spatial coherence of the two magnet vibrations for the
60 electrons and positrons, the simulated luminosity degradation induced by the
vertical vibrations is expected to be few % for both sides. Assuming no coher-
ence, the beams separation at the IP will increase up to a few times the vertical
beam sizes at the IP [3].

65 In this paper, we report the first results of an ongoing study that investi-
gates the presence and the effects of vibrations in the luminosity spectra of the

SuperKEKB collider. This approach gives preliminary indications about the sources of possible degradation effects, that could become particularly important when the collider will approach its nominal luminosity. The structure of the paper is as follow: in the next section, we introduce the mathematical tools used in the analysis of the time signals from the vibration sensors and the luminosity channels. Section 3 focuses on the description of the SuperKEKB MDI area with the position of the vibration sensors around the BELLE II detector and the acquisition setup, while the Lumibelle2 monitor is presented in Section 4. In Section 5 we analyse the vibrations and luminosity spectra, identifying and classifying the main type of disturbances in the vertical and transversal planes. The analysis helps to identify the important frequency ranges and to reveal the effects of the mechanical supports.

2. Vibration analysis technique

The vibration analysis is based on Power Spectral Density (PSD) to identify resonances hidden in the time signals. PSDs are used to quantify and compare different vibration environments. They are normalized to the frequency bin width preventing the duration of the data set (and corresponding frequency step) from changing the amplitude of the result. Vibrations are analysed using the PSD $S_z(f)$, measured in m^2/Hz , where z indicates the vertical direction (x for the transverse direction). The magnitude of the displacement can be calculated by taking the square root of the area under a PSD:

$$z_{rms}(f_{min}) = \sqrt{\int_{f_{min}}^{\infty} S_z(f)df} \quad (1)$$

Calculating this cumulative RMS is also a helpful way of seeing which frequency components are contributing most of the displacement amplitude. Another important aspect for the following analysis is the property of spatial coherence between the motion detected at two different measurement points, defined by

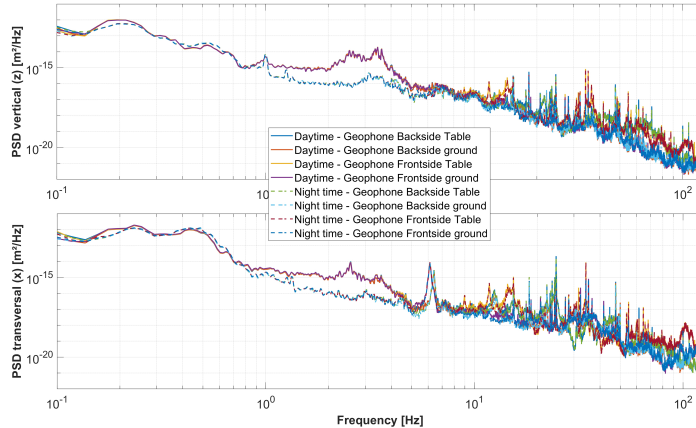


Figure 1: Day-night vertical and horizontal PSD on both sides of Belle II detector.

the modulus of the normalised cross-correlation function:

$$K(f) = \frac{\langle X(f) \cdot Y^*(f) \rangle}{\sqrt{\langle X(f) \cdot X^*(f) \rangle \langle Y(f) \cdot Y^*(f) \rangle}} \quad (2)$$

95 where $X(f)$ and $Y(f)$ are the Fourier transforms of the two signals. The maximum value of the coherence is equal to one and implies that the two signals have a constant phase relationship.

Fig.1 shows the day-night vertical and transversal PSD acquired on the ground on both sides of the Belle II detector. The low-frequency part of the spectra (below few Hz) is characterised by seismic motions such as the tidal motion and micro-seismic peaks with frequencies in the range of [0.1-0.25] Hz. For frequencies above few Hz, spectra are dominated by technical noise induced by electric motors and the systems installed in the accelerator tunnel, and by cultural noise from road traffic nearby, railways and industry. The plot also indicates a difference of vibration levels during the day with the presence of higher peaks in amplitude.

100
105

3. SuperKEKB MDI area and vibration measurement setup

The relatively large beam crossing angle at SuperKEKB of 83 mrad is motivated in the context of the *nanobeam* scheme by the need to make the effective

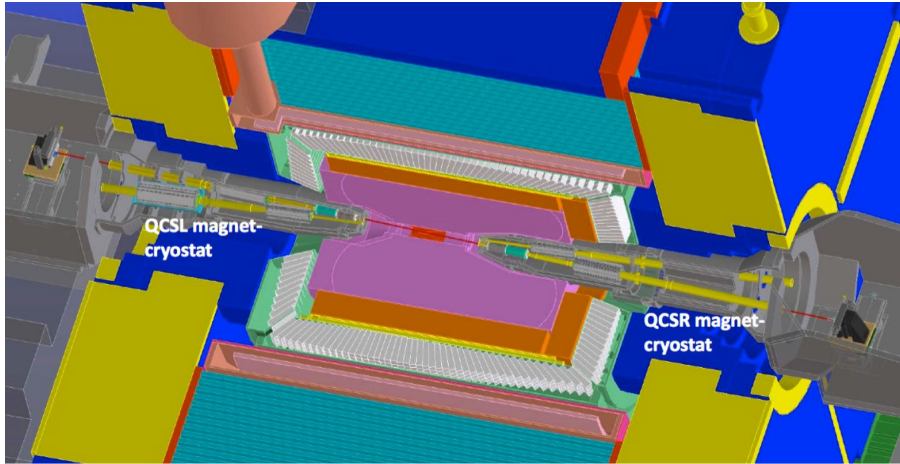


Figure 2: Machine Detector Interface area with SC final focus quadrupoles inside cryostats.

110 luminous region at the collision point much shorter than the equilibrium bunch-
 length values in each of the rings, in order to enable reducing the β_y parameter
 without limitations from the hour-glass effect, and thereby achieve a large in-
 stantaneous luminosity. The constraints from the independent magnet designs
 for each beam, from the optics of the interaction region and the backgrounds
 115 from radiation are also taken into account. The interaction region area is rep-
 resented in Fig.2 with the two cryostats and their first final focus quadrupoles
 inside the Belle II detector. We can notice the different sizes of the magnets for
 the electron and positron beams, due to their different energies, needed to gener-
 ate a Lorentz boost for the produced B-meson pairs, e.g. to allow measurements
 120 of lifetimes.

The vibration analysis has been realised using two tri-axial geophones from
 Guralp T6 (CMG-6T), a CompactRIO Controller cRIO-9022 designed by Na-
 tional Instruments together with two 24-Bit, 4-Channel Voltage Input Modules
 (NI 9239). A sampling frequency of 250 Hz has been chosen because of the
 125 relatively low frequencies of the ground motion involving relevant amplitudes.

The CMG-6T sensors (see Fig.3) are highly sensitive electromagnetic geo-
 phones measuring velocity in 3 directions (one vertical and two horizontal).

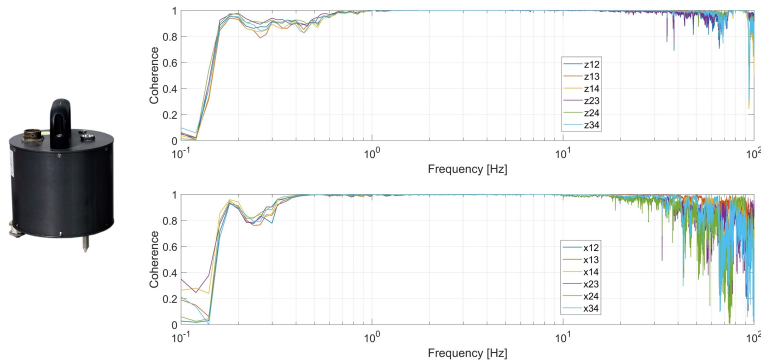


Figure 3: A CMG-6T sensor and the coherence of two of these geophone sensors side by side.

They have a flat frequency response from 0.03 Hz to 100 Hz. The actual operating range is however closer to [0.3 - 100] Hz as their internal noise at low
 130 frequency is rather high when the ground velocity is very low. A preliminary study was performed to ensure that the sensors behave correctly and were able to measure in the bandwidth of interest (depending on the site). The coherence measurement between geophone sensors placed side by side is represented in Fig.3. The upper plot gives the vertical coherence of the ground motion of the
 135 four sensors located side by side, while the lower plot gives the transversal coherence of the ground motion. These results demonstrate that, with a coherence of almost 1, the geophones are suitable to perform measurements in the range [0.3 - 100] Hz.

3.1. *Vibration source identification and sensors location*

140 Four sensors have been installed near the Belle II detector providing long-term monitoring of seismic motion and cultural noise in the vertical and transversal direction. They allow the identification of disturbances or specific events. Each event is mentioned in a weekly report available on the LAPP website [9]. An example presented in Fig.4 shows how disturbances are identified. The plot
 145 is a spectrogram of the ground motion PSD (measured in the vertical direction) with some typically observed events. Indeed, the SuperKEKB experiment is often disturbed by seismic events that our sensors detect, as highlighted in the

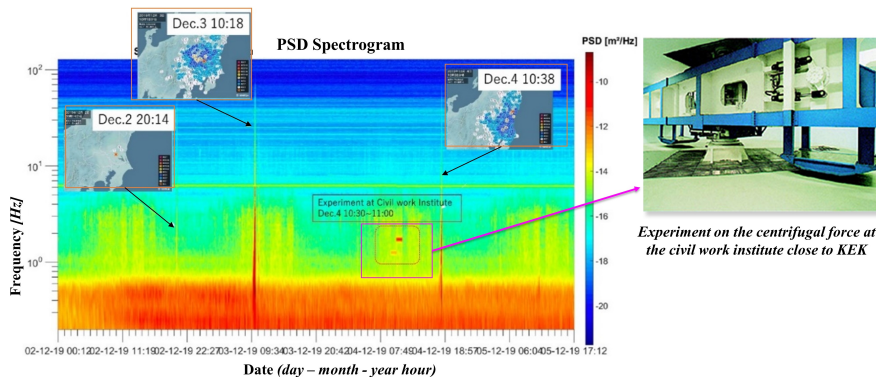


Figure 4: Vibration analysis: earthquake and external perturbations.

figure by images showing the location-time of the seismic event. An initially
 unknown disturbance source was also regularly observed to cause luminosity
 150 disturbances in the low-frequency range [1:2]Hz. As illustrated in Fig.4, the
 disturbance was confirmed by the ground motion measurements and the source
 was identified. It is a centrifugal force generator experiment (a rotating arm of
 6,6m long, 50G) at a civil work institute located close to the KEK site. The
 main goal of the experiment is to test various materials and structures used for
 155 building but, unfortunately, it generates important disturbing vibrations to the
 SuperKEKB collider.

The CMG-6T sensors are placed inside protection boxes made with mu-metal
 and lead against radiation and magnetic fields. The positions of the four sensors
 are indicated in Fig.5. Two sensors are located at each side of the detector called
 160 frontside (sensors A and B) and backside (sensors C and D). Two are standing
 on the ground (A and C) while the others stand on the support of the cryostat (B
 and D).

4. LumiBelle2 setup and measurements

The fast luminosity monitor LumiBelle2 is based on sCVD diamond sen-
 165 sors installed on both sides of the IP in LER and HER beamlines, to measure
 Bhabha scattered positrons and photons, respectively[4]. The system provides

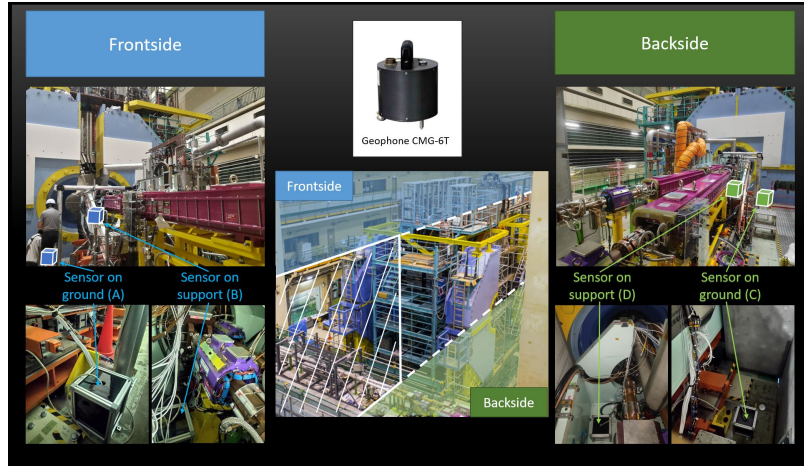


Figure 5: Location of the 4 geophones in the SuperKEK experiment.

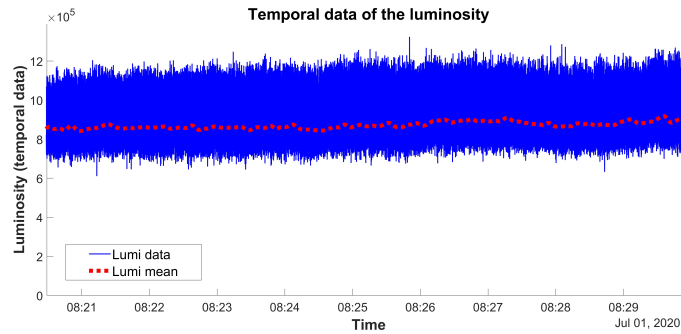


Figure 6: Example of luminosity temporal signal at 1 kHz.

integrated luminosity signals at 1 kHz as input for the horizontal dithering feed-
 back system [3] as well as luminosity signals at 1 Hz, both integrated and per
 170 beam currents and checks of possible luminosity variations along the bunches,
 respectively.

For an ideal head-on collision, the luminosity of a collider depends only on
 the beam intensities, the horizontal and vertical beam sizes, the number of
 175 bunches and the revolution frequency. If the beams are colliding with an offset,

the luminosity is reduced by a factor easily computed by folding the two transverse distributions, usually assumed to be Gaussian. In the case of SuperKEKB with its *nanobeam* scheme and large horizontal crossing angle, the computation for horizontal offsets must also take into account the small vertical β at the IP.

180 More generally, a realistic computation should also include beam size distortions at the IP due to linear and non-linear optical aberrations, as well as beam blow-up from the beam-beam interaction. In the presence of time-dependent disturbances of transverse offsets and other parameters, one can expect the luminosity to vary over time, as shown in Fig.6 where the solid line is a typical

185 measurement at 1 kHz of the luminosity, and the dotted line is the previous measurement after filtering to remove fast perturbations and obtain the average behaviour. The disturbances at different time scales come from various sources such as position jitter of the beams at the IP arising from mechanical vibrations, transient betatron oscillations arising from imperfect continuous horizontal in-

190 jections, a fraction of which coupling into the vertical plane due to misalignments, and getting corrected at least partly by the beam-beam deflection based feedback system, as well as from other beam dynamics effects.

5. Analysis of vibrations and luminosity spectra

Vibration sources can be classified according to their coherence. For example, Fig.7 shows a measurement in the transverse direction on points A, B, C

195 and D, corresponding to the sensor locations described in Fig.5. M_X indicates the motion at a generic point X .

Three main types of disturbances could be observed and selected as following:

- Type P1: Coherent at both sides of the detector and not amplified by the

200 mechanical assembly: $M_A = M_B = M_C = M_D$

- Type P2: Not coherent at both sides and not amplified by the mechanical assembly: $M_A = M_B \neq M_C = M_D$

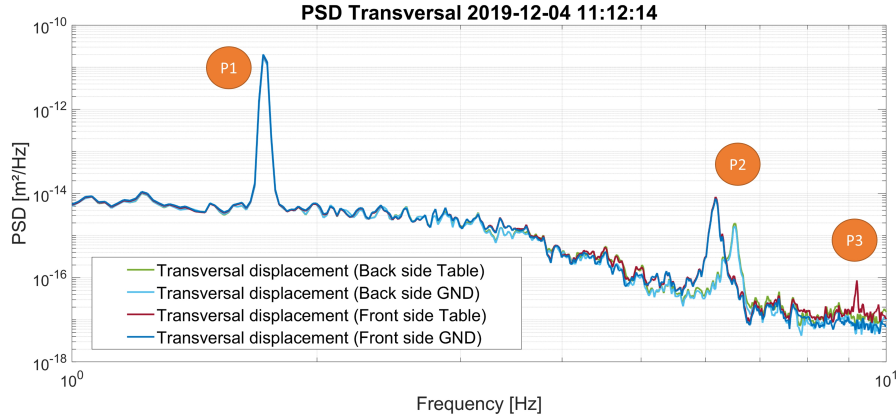


Figure 7: Transverse PSD from the four seismic sensors.

- Type P3: Resonance modes of the cryostat or of the cryostat support:
 $M_A = M_C = M_D \neq M_B$ or $M_A = M_B = M_C \neq M_D$

205 The effect induced by the third type of disturbance is the most important for this study. Indeed, for such experiments, the high sensitivity of the final focus system to vibrations is one of the main factors degrading the beam interaction efficiency at the IP. This is particularly important for SuperKEKB where the Final Focus (FF) magnets are integrated into two cantilever cryostats, inside
 210 the Belle II detector. The specificity of this setup is that the two face-to-face cryostats are not identical and the HER and LER magnets are not at the same position inside the cryostat as described in Fig.8.

The displacements of the magnets in the collider are the product of their excitation through ground motion and cultural noise by the transfer function of
 215 the mechanical assembly which supports them and in which they are integrated. Fully evaluating the effects on the collider performance requires deep knowledge of the behaviour of a relatively complex mechanical system. Since the ground motion measured on site decreases quickly with frequency and given the main observed resonance modes of the cryostat, only the frequency range [1 50] Hz
 220 is studied.

The first stage in the mechanical design of the final focus system was the

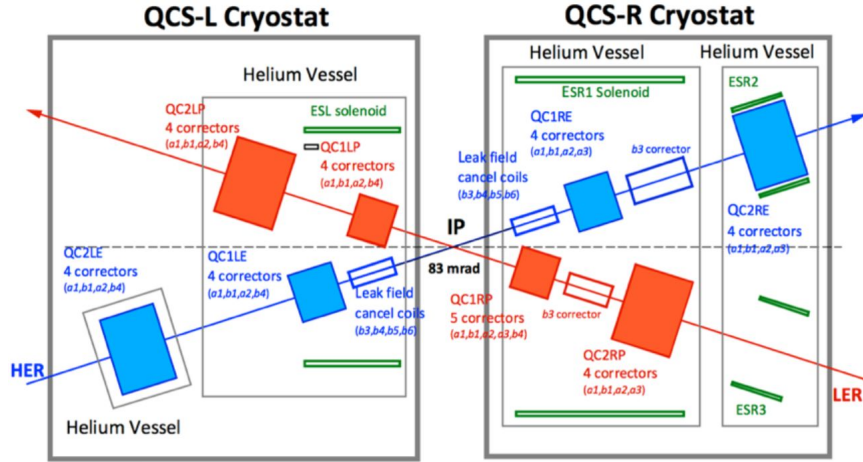


Figure 8: Elements and their position inside the final focus cryostats. Credit figure [10].

modelling of the cryostat mechanical assembly, to identify its vibration modes [2]. The presented approach is dedicated to the front side of the detector which presents the resonance modes at the lowest frequencies. The study highlighted the first two modes of flexion in the relevant bandwidth at about the same

225

frequency in the two directions due to the relative symmetry of the mechanics. To complete this theoretical approach, two campaigns of measurements were performed. The first, carried out at the beginning of the mechanical assembly, confirmed the theoretical models [2].

230

The second campaign was done in 2018 just before the insertion of the cryostat inside the detector, and therefore with a setup closer to the final one as shown in Fig.9. These measurements confirmed the previously identified resonance modes (Fig. 10) but also revealed that additional peaks appeared on the cryostat support itself.

235

One can hence consider that the first flexion mode is at about 15 Hz for the front side cryostat, and at about 24 Hz for the backside cryostat. In beam operation with the final focus magnets inside the detector, it is not possible to have such sensors on the cryostat. The closest available location is therefore on the cryostat support (Fig.5).

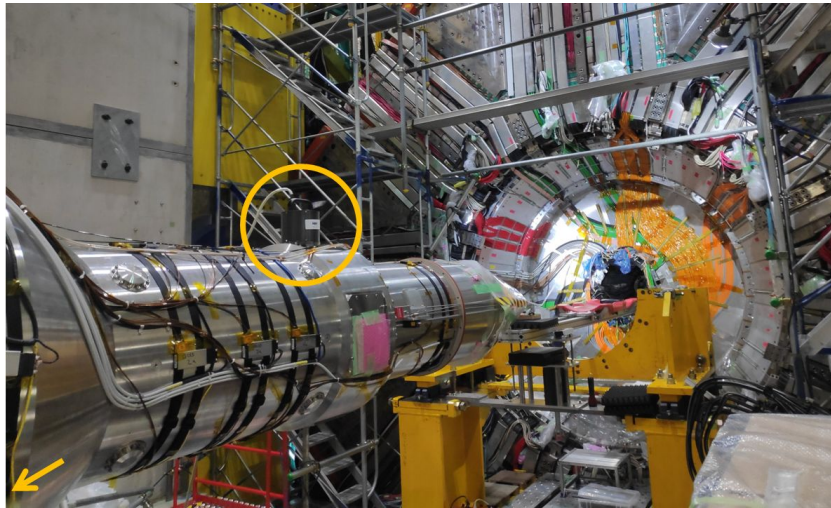


Figure 9: Picture of the cryostat outside the detector during vibration measurements performed on the ground (location indicated by the arrow) and on top of the cryostat (encircled sensor).

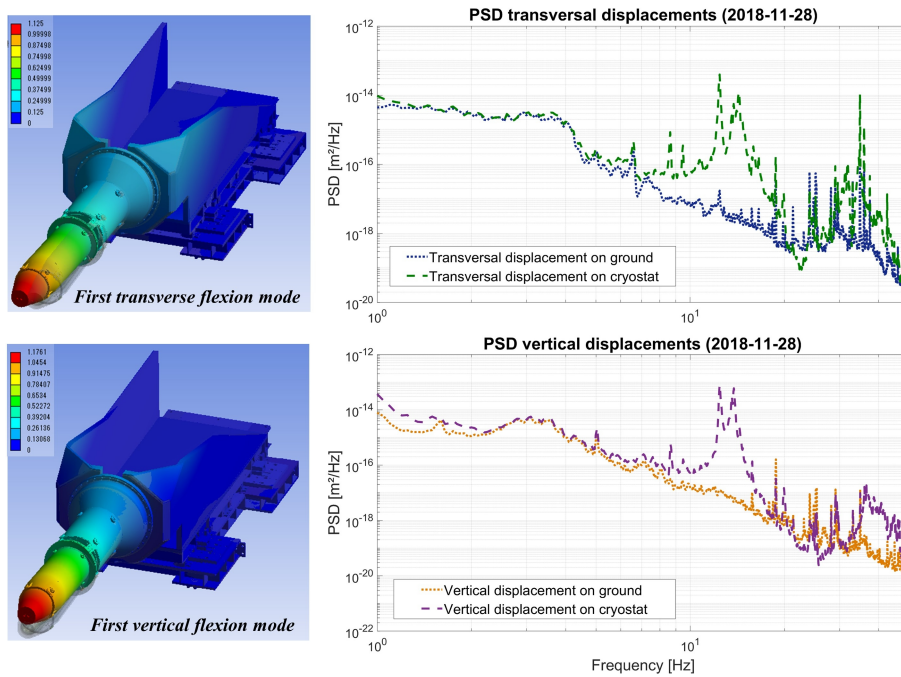


Figure 10: Vertical and transverse first flexion modes of the cryostat (left) and vertical and transverse PSD measured on the ground and on the cryostat outside the detector (right).

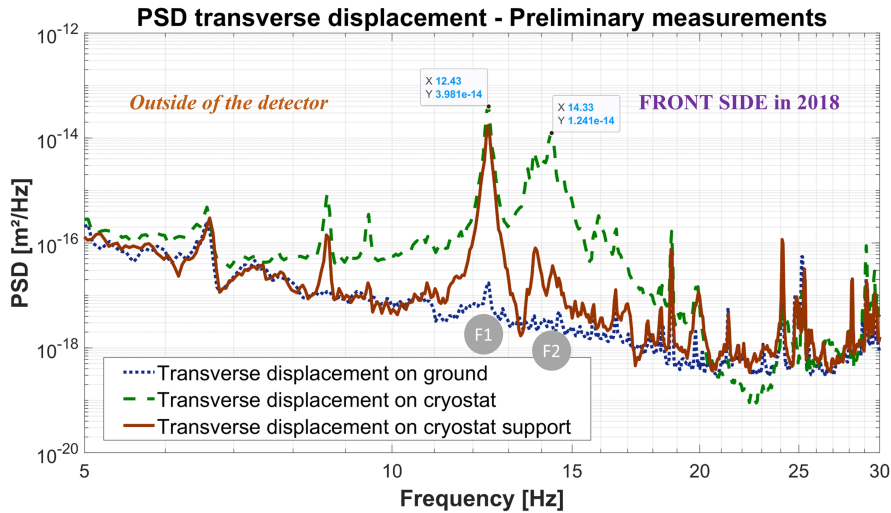


Figure 11: Transverse PSD measured on the ground, on the cryostat support and on the cryostat during vibration measurements.

240 Fig.11 and Fig.12 compare the transverse displacements measured with the cryostat outside and inside the detector. The frequency peak at (F1) location in the plot is due to a support eigenfrequency whereas the one at (F2) is the amplification of the ground motion by the first mechanical mode of the cryostat.

245 These successive measurements allow us to point out two fundamental aspects. First, the cryostat support is not rigidly fixed. Indeed, the cryostat is a cantilever structure so if the support were stiff enough, the motions of the ground and of the cryostat support would be equal. One can observe that it is not the case, the cryostat support motion is also amplified, which means that it is not only the cryostat that bend out of shape (flexion mode) but the whole assembled structure (cryostat and its support).
 250 Second, the setup has changed between the two measurements. The cryostat was moved on its support to be inserted inside the detector and the final adjustments have been done such as the connection of the beam pipes. Even if the frequencies of the resonance modes have shifted a little bit, these offsets are not very significant. Therefore,
 255 thanks to these current indirect measurements on the cryostat supports, we are

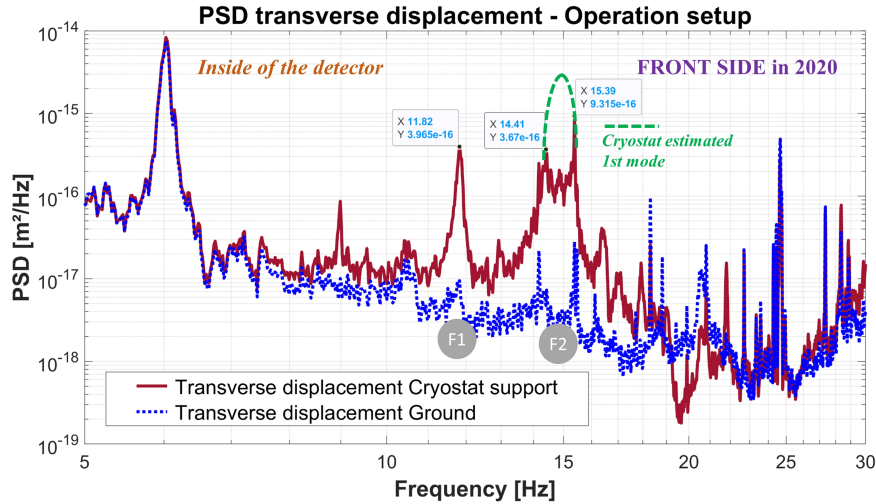


Figure 12: Transverse PSD measured on the ground and on the cryostat support during beam operation.

able to estimate the frequencies of the various cryostat resonance modes in the frequency range of interest as it is illustrated in these two figures.

Among these mechanical amplifications created by the resonance modes, the first flexion mode is the most relevant and will create the most important FF magnet motion. As mentioned before, the peculiarity of the SuperKEKB cryostat is that the FF magnets in the HER and LER beamlines are not at the same longitudinal positions, so the induced displacements will be different for each magnet. In this way, the amplitudes of the orbit distortions generated on both beams will be different and they will not fully compensate each other.

To evaluate this, our analysis is focused on the dynamic part of the luminosity signals. Fig.13 shows a PSD of the luminosity during one of the last days before the beam shutdown in summer 2020 when the peak luminosity was at the highest level.

The luminosity signal is analyzed for three main different bandwidths (B1, B2 and B3):

- B1 [0,3-10] Hz: in this bandwidth, there are no corresponding amplifications due to the mechanics. This means that the movement of the ground

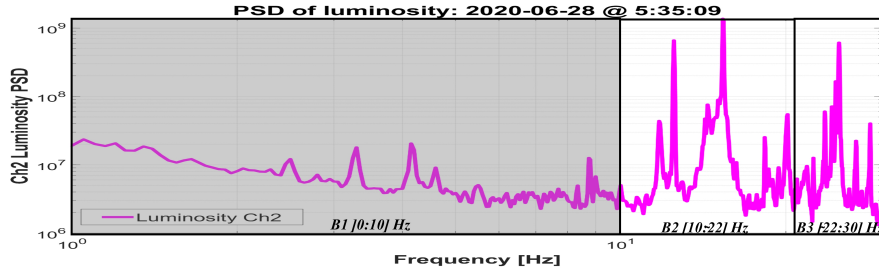


Figure 13: PSD of the luminosity on the studied bandwidths.

is equal to the movement of the cryostat support. There are therefore no differential movements between the FF magnets (plotted only above 1 Hz).

275

- B2 [10-22] Hz: this bandwidth corresponds to the first modes of the mechanical assembly at the front side of the Belle II detector.
- B3 [22-30] Hz: this bandwidth corresponds to the first modes of the mechanical assembly at the backside of the Belle II detector.

280

The B2 and B3 frequency bandwidths are the most important for this study. Fig.14 presents the analysis of data taken on the 28th of June 2020. The first row gives the PSD of the luminosity time signal, the second one the vertical displacements (ground and support) and the third one the transverse displacements (ground and support). The left column is a focus on B2 bandwidth (frontside detector for the vibration aspects) and the right column is a focus on B3 bandwidth (backside detector for the vibration aspects). Some peaks on the luminosity PSD come from external sources, especially from the beam injection, at 12.5 Hz and 25 Hz. They will therefore not be taken into account for these comparisons.

285

290

The pattern of the luminosity PSD corresponds to the pattern of the cryostat support displacement PSD, especially the frontside support for B2 bandwidth and the backside support for B3 bandwidth. To evaluate the relevance of this matching, it is useful to identify the largest values of the PSD of vertical dis-

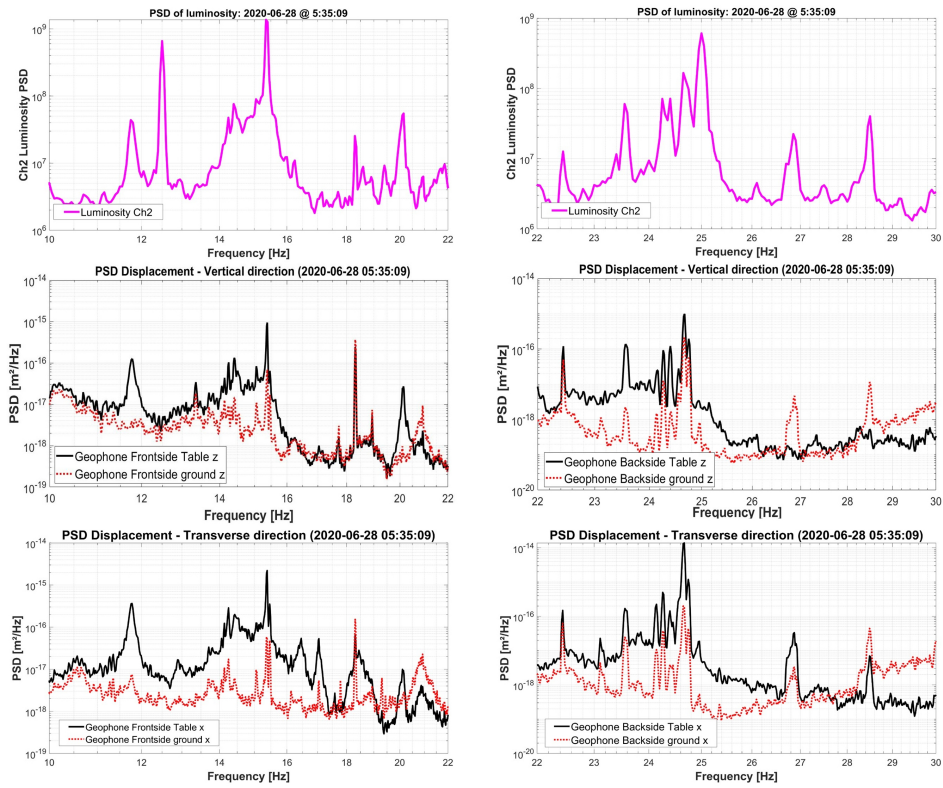


Figure 14: PSD of luminosity and PSD from all seismic sensors both in the vertical and transverse direction in the two bandwidths of interest: B2 [10-22] Hz (left column) and B3 [22-30] Hz (right column).

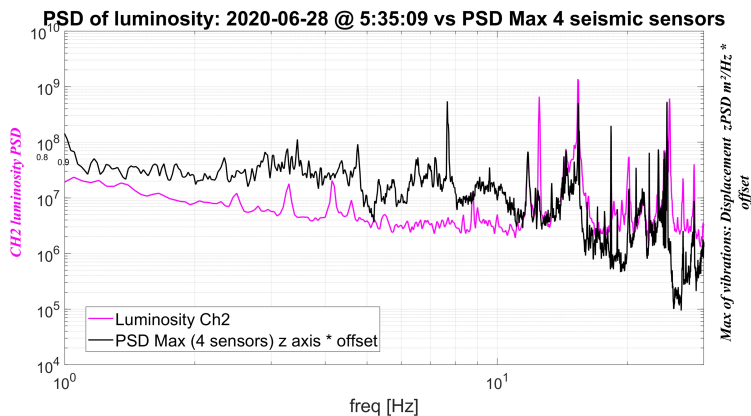


Figure 15: Comparison between the PSD of luminosity and the PSD^{max} (z axis) of the four sensors A, B, C and D on B1 bandwidth [1-10] Hz.

placement between the four measured movements M_A, M_B, M_C and M_D :

$$z_{PSD^{max}} = \text{Max}(PSD_z[M_A, M_B, M_C, M_D]) \quad (3)$$

295 This analysis was performed on the vertical axis because of the higher sensitivity to vibration in that direction due to the very flat shape of the beam.

In Fig.15 and Fig.16, the maximal vertical displacement PSD is scaled by an arbitrary factor for a better visual comparison. In the low-frequency range of
 300 Fig.15, we observe no correspondences between luminosity peaks and vibration peaks. Two aspects explain this result. First, at low frequency the coherence among the measurement points in the MDI area is high because the ground at the two sides of the detector is moving in phase with the same amplitude. Second, there is no mechanical amplification due to support or assembly which
 305 creates differential motions between the focusing elements. This result confirms that the final focusing magnets are moving with the same amplitudes. As consequence, the induced deflections of the two beams are equivalent with no perturbation of the luminosity.

In the higher frequency range of Fig.16, two major peaks in the luminosity
 310 at 12,5 Hz and 25 Hz are identified. They are induced by the top-up injection

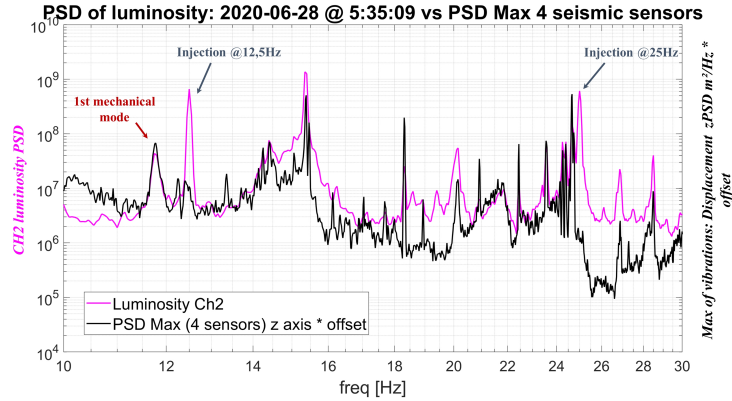


Figure 16: Comparison between the PSD of luminosity and the PSD^{max} (z-axis) of the four sensors A, B, C and D on the B2 and B3 bandwidths [10-30] Hz.

process which is not the subject of this study and completely independent from the vibrations issues. However, on these bandwidths B2 and B3, the comparison highlights that all the vibrations peaks have a direct impact on the luminosity of the collider. Indeed, each peak in the displacement PSD has its equivalent at the same frequency on the dynamics part of the luminosity PSD.

It should be noted that the main peaks correspond to the two first flexion modes of both cryostats: about 15 Hz for the front side and about 24 Hz for the backside. The reason comes from the fact that the two cryostats transfer functions generate the most important differential displacements between the final focusing magnets, and so different deflections between the HER and the LER beams.

To analyze in more details the B2 bandwidth (which stands on the best-known side thanks to the preliminary measurements), we present in Fig.17 a comparison between the luminosity PSD and the ratio of the cryostat support displacement PSD to the ground motion displacement PSD in the vertical and the transverse direction. These two last PSDs were scaled to be compared with the luminosity PSD. The black line is the PSD ratio in the vertical direction and the dotted line in the transverse direction.

The PSD ratio of the support displacements and the ground motions gives

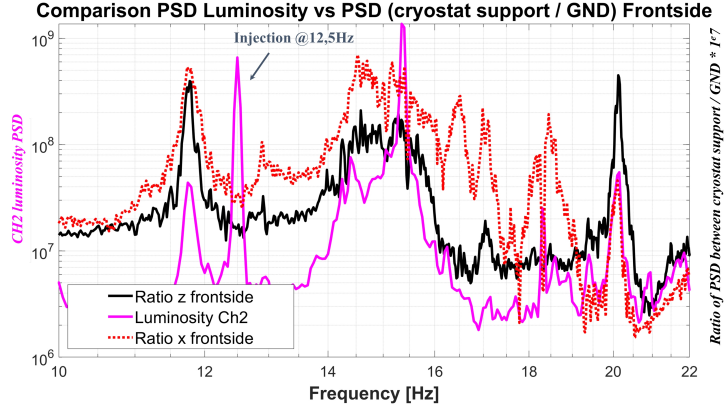


Figure 17: Comparison of the luminosity PSD respect to the ratio of the vertical and transverse directions PSD on the frontside.

330 an estimation of the sources of the disturbance, which could create differential motion between both sides of the detector (transfer functions, local sources, etc.). Indeed, even if it is an indirect measurement which does not allow to evaluate the final focus magnets motion inside the cryostat, especially their amplitudes, the main frequencies of interest are identified by taking into account
 335 the flexibility of the assembly.

Except for the peak due to the injection at 12.5 Hz, Fig.17 highlights that all peaks of the luminosity PSD come from the differential motions between the ground and the cryostat support in the vertical direction (peaks in the vertical displacement ratio PSD, black line). It should also be noted that the transverse
 340 direction reveals less importance due to the larger size of the beam in this direction.

6. Conclusions

From our analysis, we conclude that vibrations impact the temporal evolution of the luminosity of the SuperKEKB collider. As expected from beam
 345 sizes, the effect of vibration is more pronounced in the vertical direction. Moreover, the correspondences among luminosity and vibration spectra are very close

in the frequency range of [10-30] Hz which contains the two main first flexion modes of both cryostats. These results are particularly important given that the machine is not at the nominal luminosity of $6 \times 10^{35} \text{cm}^{-2}\text{s}^{-1}$ yet. With the
350 increase of the luminosity towards the nominal value and, hence, smaller beam sizes at the interaction point, the impact of vibrations may increase.

- [1] Y. Ohnishi, et al., Accelerator design at superkekb, Progress of Theoretical and Experimental Physics 2013 (3). doi:10.1093/ptep/pts083.
- [2] H. Yamaoka, et al., The mechanical and vibration studies of the final focus magnet-cryostat for superkekb, in: 5th International Particle Accelerator Conference, 2014, p. THPRI005. doi:10.18429/JACoW-IPAC2014-THPRI005.
355
- [3] Y. Funakoshi, et al., Interaction Point Orbit Feedback System at SuperKEKB, in: 6th International Particle Accelerator Conference, 2015, p. MOPHA054. doi:10.18429/JACoW-IPAC2015-MOPHA054.
360
- [4] C. G. Pang, et al., A fast luminosity monitor based on diamond detectors for the superkekb collider, Nuclear Instruments and Methods in Physics Research Section A 931 (2019) 225–235. doi:10.1016/j.nima.2019.03.071.
- [5] T. Hirai, et al., Real-time luminosity monitor for a b-factory experiment, Nuclear Instruments and Methods in Physics Research Section A: Accelerators, Spectrometers, Detectors and Associated Equipment 458 (2001) 670–676. doi:10.1016/S0168-9002(00)00766-X.
365
- [6] M. Masuzawa, J. W. Flanagan, Y. Funakoshi, K. Oide, IP orbital feedback for collision tuning at KEKB, in: 7th European Particle Accelerator Conference (EPAC 2000), 2000, pp. 1211–1213.
370
- [7] A. Fisher, et al., Commissioning the fast luminosity dither for pep-ii, 2007 IEEE Particle Accelerator Conference (PAC) (2007) 4165–4167. doi:10.1109/PAC.2007.4440072.

- 375 [8] M. Masuzawa, et al., Early Commissioning of the Luminosity Dither
Feedback for SuperKEKB, in: 7th International Beam Instrumentation
Conference, JACoW, 2019, p. TUPC13. doi:10.18429/
JACoW-IBIC2018-TUPC13.
- [9] SuperKEKB vibration measurement analysis, [https://lappweb.in2p3.
380 fr/SuperKEKB/](https://lappweb.in2p3.fr/SuperKEKB/).
- [10] N. Ohuchi, et al., Design of the superconducting magnet system for the
superkekb interaction region, Proceedings of the NA-PAC13, Pasadena,
CA USA (2013) pp.759-761.
URL <https://jacow.org/pac2013/papers/weoda1.pdf>